

3D Shape Description of the Bicipital Groove of the Proximal Humerus

Aaron D. Ward¹, Mark E. Schweitzer², and Ghassan Hamarneh¹

¹Simon Fraser University, School of Computing Science, Burnaby, BC V5A 1S6, Canada;

²Department of Radiology and Orthopedic Surgery, NYU School of Medicine, Hospital for Joint Diseases, New York, NY 10016, U.S.A.

1. ABSTRACT

Bicipital root and proximal tendon disorders are an important symptom generator in the shoulder. The accuracy of the diagnosis of many shoulder disorders visually without quantitative shape analysis is limited, motivating a clinical need for some ancillary method to access the proximal biceps. Because of the known inter-relationship of the bicipital groove (BG) with several types of disorders, we propose an approach to the 3D shape description of the BG that captures information relevant to disorders of the shoulder (e.g. width, depth, angles of walls, presence of spurs). Our approach is medial-axis based and captures intuitive aspects of shape such as thickness, bending, and elongation. Our proposed method overcomes the well-known problem of boundary sensitivity in the medial representation as it is applied to representation and analysis of BG shape. We give preliminary quantitative results indicating that this representation does capture shape variation within our experimental data, providing motivation to explore more sophisticated statistical analysis based on this representation in future work. We also provide a method for semi-automatic segmentation of the BG from computed tomography (CT) scans of the shoulder; an important precursor step to BG shape analysis.

2. INTRODUCTION

The bicipital groove of the proximal humerus (hereinafter referred to as the BG) is located on the head of the humerus. The long biceps tendon is located in this groove; the BG serves to keep the tendon in place as the arm moves. Bicipital root and proximal tendon disorders are becoming increasingly recognized as an important symptom generator in the shoulder. The spectrum of abnormalities includes synovitis, pulley lesions, SLAP tears, biceps dislocations and proximal tears.² Historically, the accuracy for the diagnosis of many of these disorders by imaging has been limited. Therefore, there is a clinical need for some ancillary method to access the proximal biceps. Because of the long known inter-relationship of the BG with several types of shoulder disorders, this is an obvious source of secondary data.² Currently, most BG shape analysis is fairly primitive and obtained from non-tomographic (2D) radiographs.^{2, 11–14, 18} We are therefore motivated to develop a rich, 3D means of describing and analyzing BG shape.

The objective of this work is to provide a 3D shape representation that allows for effective statistical analysis of anatomic shapes relevant to musculoskeletal disorders, where the results of such analysis are intuitive to the clinician. Medical research indicates that for the BG, such a shape description should capture the depth, width, presence of spurs (bony protrusions inside the BG), presence of the supratubercular ridge of Meyer,¹⁰ and angles of both the medial and lateral walls of the BG.² Our chosen representation is inspired by the medial axis representation, originally motivated by Blum's medial axis transformation,³ and more recently investigated by many others.^{1, 8, 15, 16, 21} Medial axis-based representations capture shapes as measured thickness values, relative to some medial geometry (e.g. a medial axis in the 2D case; a medial sheet in the 3D case). A medial representation is an attractive choice for this clinical application because thickness values computed relative to the medial sheet capture clinically relevant measurements^{2, 6, 10, 12, 23} (e.g. depth, width, wall slopes) directly. It is well known that medial representations tend to be unstable with respect to small changes in the object

Further author information: (Send correspondence to A.D.W.)

{A.D.W., G.H.}: E-mail: {award, hamarneh}@cs.sfu.ca, WWW: <http://www.cs.sfu.ca/>
M.E.S.: E-mail: mark.schweitzer@nyumc.org, WWW: <http://www.med.nyu.edu/>

boundary. We overcome this problem by fixing the topology of the medial sheet and determining its precise shape and position according to a criterion which maximizes both sheet smoothness and medialness.

In section 3, we review relevant work from the medical literature in order to motivate the need for BG shape description, and to determine the important aspects of BG shape that need to be described. In section 4 we examine the nature of the data sets containing bicipital grooves whose shapes we wish to describe, and in section 5 we explore the details of our approach to solving the problem. In section 6 we discuss the experimental results. Finally, we summarize this work and give indications of future research directions in section 7.

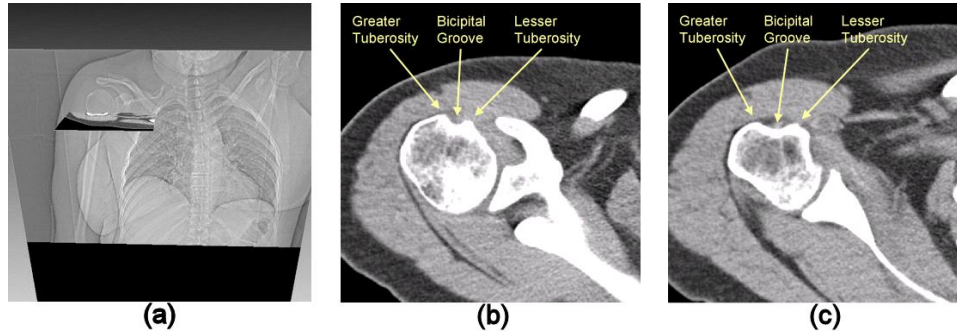


Figure 1. (a) Perspective view of one of the shoulder data sets. Axial slice shows the position of the BG. (b) The BG lies between the greater and lesser tuberosities. (c) A distal slice illustrating the variability of the shape of the BG.

3. RELATED WORK

Research into the measurement of the BG and the correlation of these measurements to the incidence of malady has been ongoing for several decades. Before examining this research, we briefly review relevant shoulder anatomy. Figure 1(b) and (c) show axial slices of the shoulder. The humeral head contains the BG, which is the groove between the greater and lesser tuberosities, indicated with arrows on the figure. The lesser tuberosity is also known as the medial tuberosity; it is closer to the vertical center line of the body than is the greater tuberosity.

We examine major medical research developments in BG shape measurement in chronological order. In 1928, Meyer described the significance of the supratubercular ridge, which is a ridge of bone, projecting immediately proximal to the medial wall of the BG and continuous with it. The supratubercular ridge is not present in all humeri; Meyer cites a study of 200 humeri of which it appeared in 17.5%. The presence of the supratubercular ridge has been demonstrated to increase the probability of dislocation of the biceps tendon from the BG.¹⁰

Hitchcock and Bechtol⁶ in 1948 studied 100 humeri, and in doing so they distinguished between ‘marked’ and ‘moderate’ development of the supratubercular ridge. Their finding was that the ridge was markedly developed in 8% of the humeri, and moderately developed in 59%. They also found that of the humeri showing a supratubercular ridge (markedly or moderately developed), 45% showed spurs, whereas of the remaining humeri, only 3% showed spurs. Hitchcock and Bechtol also noted the importance of the angle of the medial wall (to the line joining the greater and lesser tuberosities) of the BG formed by the lesser tuberosity. The anatomy of the human shoulder dictates that when the biceps tendon is under tension, it is pulled against the lesser tuberosity. The angle of the medial wall is therefore very important in retaining the tendon in the BG; a steeply sloping medial wall will offer better retention. Hitchcock and Bechtol took measurements of this angle, quantized to 15 degree increments, and found the following distribution, which give a sense of the expectation for a normal BG: 10%, 35%, 34%, 13%, 6%, and 2%, for 90°, 75°, 60°, 45°, 30°, and 15°, respectively.

In 1973, O’Donoghue¹² examined BG shape in athletes, with the objective of determining the relationship between BG shape and incidence of injury in sports. His work shows that a BG with a medial wall angle of 90° may restrict the movement of the long biceps tendon and increase the incidence of tenosynovitis. At the other extreme, angles of 45° may be tolerable under low stress, and angles of 30° and 15° will favour dislocation of the tendon from the BG.

Bateman² in 1978 states that BG depth and width are important factors in the retention of the long biceps tendon. A thick tendon in a wide, shallow BG will have a tendency to dislocate. At the other extreme, a deep, narrow groove is likely to constrict the tendon and cause irritation. It is also noted that formation of spurs in the BG may result in the fraying of the tendon. For further reading on medical analysis of BG shape, several other works may be consulted.^{4, 11, 13, 14, 18, 20, 22-24}

A literature search reveals that to the best of our knowledge, there is little or no current work on 3D shape description of the BG of the proximal humerus. Current BG shape descriptions (such as that described in¹⁴) are typically 2D, taken from a single axial slice, and consist only of a few measured angles, widths, and depths (figure 2). These measurements are insufficient because they may reveal information only about the single cross section which they measure; problems present in another part of the BG (e.g. spurs) may be missed. We are therefore motivated to develop an approach to 3D shape description that allows measurement of the following attributes: depth, width, spurs, supratubercular ridge, and angles of the BG walls.

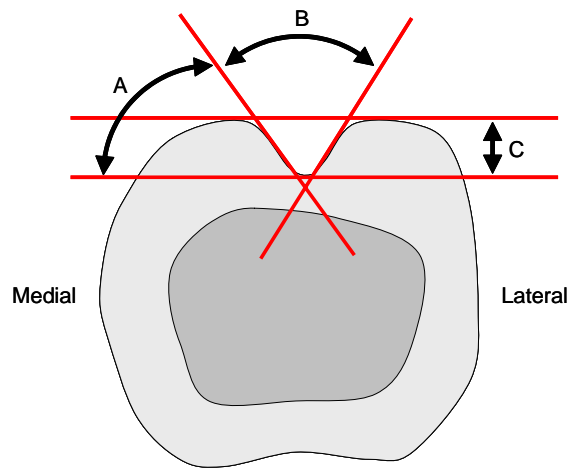


Figure 2. Diagram of an axial cross section of the humerus in standard anatomical position depicting the BG indentation on top. A, B, and C indicate measurements of the BG used in many previous works (adapted from¹⁴). A: The medial opening angle. B: The total opening angle. C: The depth of the BG.

4. MATERIAL

The data sets consist of 38 MR and CT scans of the shoulder, with the humerus approximately axially aligned within the data sets. A perspective view of one such data set is given in figure 1(a). This figure shows a radiograph of the subject on which the scan was performed, to place in anatomical perspective the position of the humeral head containing the BG (shown in the smaller intersecting axial slice). Figure 1(b) and (c) are axial CT slices showing the BG; note the difference in BG curvature between these two figures. This difference in BG shape in two cross sections from the same subject illustrates the need for 3D shape description that integrates measurements taken throughout the entire groove, rather than relying on a single 2D cross section.

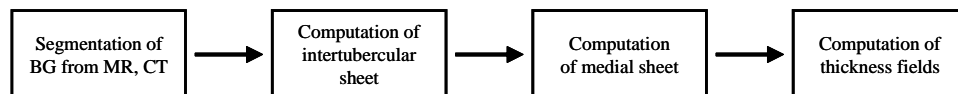


Figure 3. Flowchart describing the overall process of computing the shape description for the bicipital groove.

5. METHODS

The overall process followed in computing our description is described in the following sections (figure 3):

5.1. Segmentation of the BG

We begin by segmenting the BG from a 3D image of the shoulder. The segmentation technique used is not a primary focus of this work, but is illustrated briefly in this paper for completeness. The segmented BG takes the form of a high resolution (isotropic voxels are 0.1mm^3 in size) binary labeled 3D image, with one label indicating the BG and the other indicating the background. Figure 4 illustrates the segmentation process used in this work. Semi-automatic segmentation of the BG from CT data is made possible by the high contrast of bone to soft tissue, as well as the concave shape of the BG on each axial slice. The user specifies the superior and inferior slices in the data set containing the BG. Within this slice range, the user selects an initial slice, and draws a rectangle that contains the groove on that slice. The process is automatic from this point forward and proceeds in a slice to slice manner. On each slice, binary thresholding (threshold = 0.5) is used to extract bone from background. The resulting image has extremely high contrast between bone and soft tissue, a Sobel filter is sufficient to quickly highlight edges where bone meets soft tissue. All edge points not lying within the user's specified rectangle are then discarded. Any further edge points not having line-of-sight to the center of the rectangle are discarded; all remaining edge points lie on the BG surface due to its concave shape. The rectangle is then translated so that its center coincides with the centroid of the remaining edge points to initialize its position on the next slice in the dataset. This operation is justified due to the fact that the bicipital groove's shape changes smoothly from one axial slice to the next. This overall process is repeated for every slice between the user's specified superior and inferior slices. Sampled points from the segmented BG are then used to interpolate a spline surface¹⁷; figure 5(a) and (b) for an example of the BG surfaces output from segmentation.

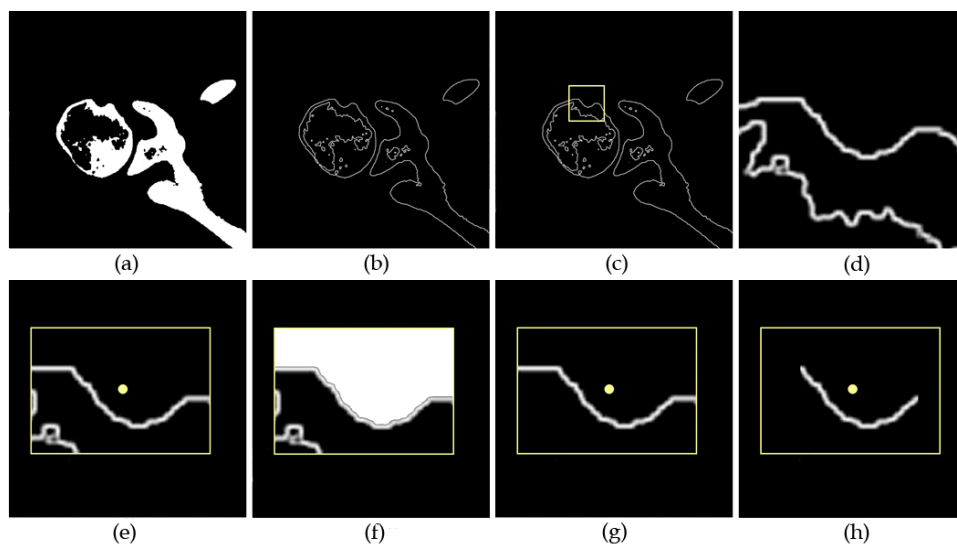


Figure 4. (a) An axial slice after binary thresholding. (b) Result of applying the Sobel gradient operator to (a). (c) An area of interest on which we will zoom in. (d) Zoomed view. (e) R and its center. We remove from consideration all edge points lying outside of R . (f) Result of region growing using the center of R as the seed. (g) Removal from consideration all edge points not touched by the region grown in (f). (h) Removal from consideration all edge points that do not have line-of-sight to the center of R .

5.2. Computation of the intertubercular sheet

The BG is formed by the greater and lesser tuberosities. On each axial cross section of the segmented BG, the endpoints of the groove appearing on that cross section correspond to the outermost points of the tuberosities. Our algorithm finds these endpoints on all BG cross sections, and then computes a sheet that passes through all of these endpoints, closing the groove. Because this sheet intersects the outermost points of both tuberosities of

the humeral head, we denote it the *intertubercular* sheet. An example is shown in figure 5(c). We define the *depth* of the BG relative to the intertubercular sheet. The depth of the BG is defined as follows: at any point P on the BG surface, BG depth at P is defined as the perpendicular distance from P to the intertubercular sheet (figure 6). This approach to BG depth is based on approaches taken in the medical literature, dating back to Meyer's relevant work in 1928¹⁰ (figure 2). It is important in defining measures such as depth and width to maintain consistency with clinical definitions of these terms.

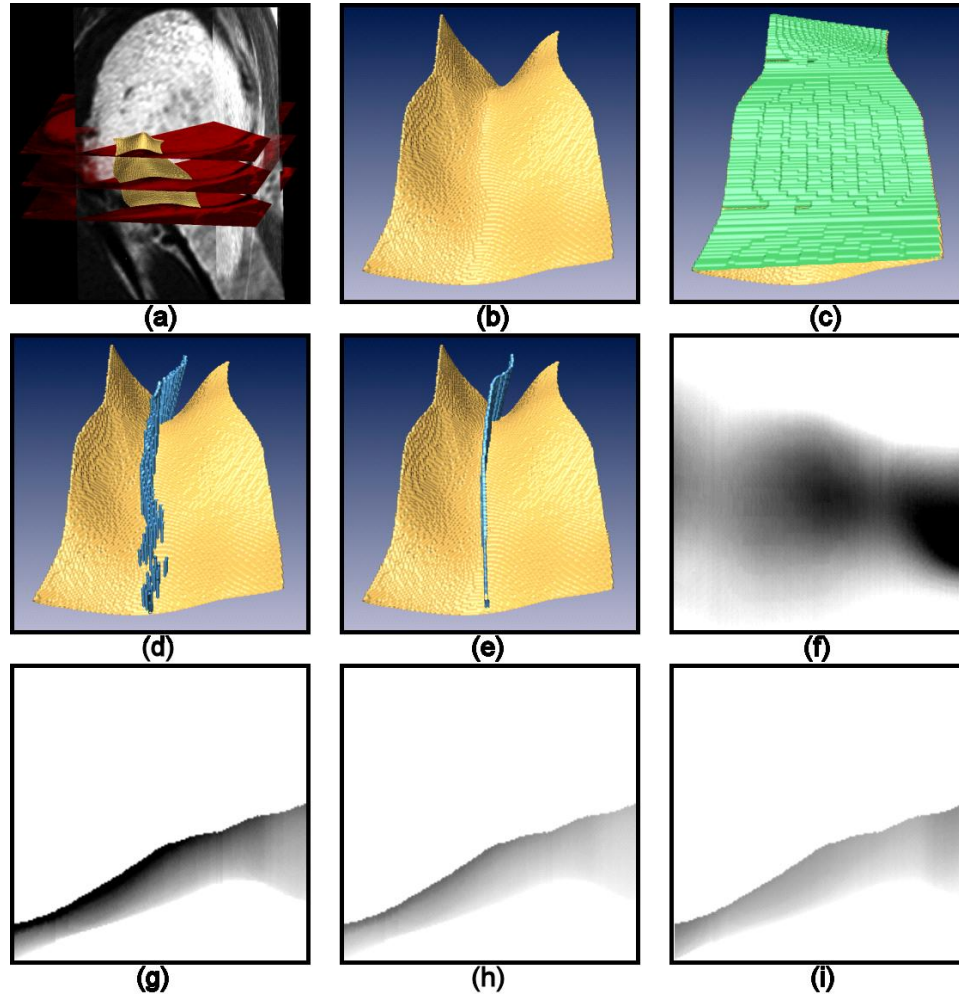


Figure 5. (a) BG visualized in context with coronal and sagittal slices (gray) and axial slices (red). (b) BG visualized out of context. (c) BG with intertubercular sheet fitted (green). (d) BG with medial sheet (blue) computed using BG depth as the only criterion. Note discontinuities. (e) BG with medial sheet (blue) computed using smoothness and depth as criteria, weighted equally. (f) Depth field. (g) Width field. (h) Lateral wall field. (i) Medial wall field. In (f) through (i), the horizontal axis of the figures corresponds to the axial dimension from the volume data set (traveling from left to right along this axis moves superior). Darker values indicate larger thickness values.

5.3. Computation of the medial sheet

When global information about a structure to be represented using a medial representation is known beforehand, it is useful to fix the topology of the medial geometry to reduce sensitivity of the medial representation to small changes in the object contour.⁵ Because the BG is known to be a trough-like structure, we fix the topology of the medial sheet to be a single, non-branching surface. The medial sheet is computed according to two criteria: medial sheet smoothness, and positioning at the deepest part of the BG on each axial slice. The medial sheet

is perpendicular to the intertubercular sheet at each axial slice, intersecting the intertubercular sheet at some point. This intersection point could be computed as the point of greatest BG depth; this is motivated by a desire to position the medial sheet along the trough so as to divide the BG in its deepest region. However, this approach makes the position of the medial sheet very sensitive to small variations in BG depth from one cross section to the next, and results in discontinuities appearing in the medial sheet (figure 5(d)). Such discontinuities will carry over into thickness fields computed based on the medial sheet, disrupting statistical analysis of the thickness fields to find anomalies in the BG walls (e.g. for the detection of spurs, which cause biceps tendon irritation and fraying). To overcome this problem, dynamic programming⁷ is used to find the optimal path along the surface of the BG. We treat the path-finding problem as a multi-stage decision problem, where there exists one stage for each axial slice of the BG. At each stage, one point must be chosen from all of the points lying on the surface of the BG at the axial slice corresponding to that stage. The objective is to find the path that, as much as possible, lies in the deepest part of the BG, but without sacrificing smoothness. The path is chosen that maximizes the following objective function at each stage:

$$Score = \alpha D + \beta S$$

Where D is the BG depth, S is the smoothness of the curve defined by the path, and α and β are tuning parameters. We obtained good results for all data sets by setting $\alpha = \beta = 0.5$. The dynamic programming method calculates the optimal path while reducing the number of computations required (as compared with a brute-force search for the optimal path). Once this path is found, the medial sheet is computed to (a) follow this optimal path, and (b) be normal to the intertubercular sheet at each point where the medial sheet intersects the intertubercular sheet. The result of this operation is shown in figure 5(e)); a continuous medial sheet positioned very near the deepest part of the groove.

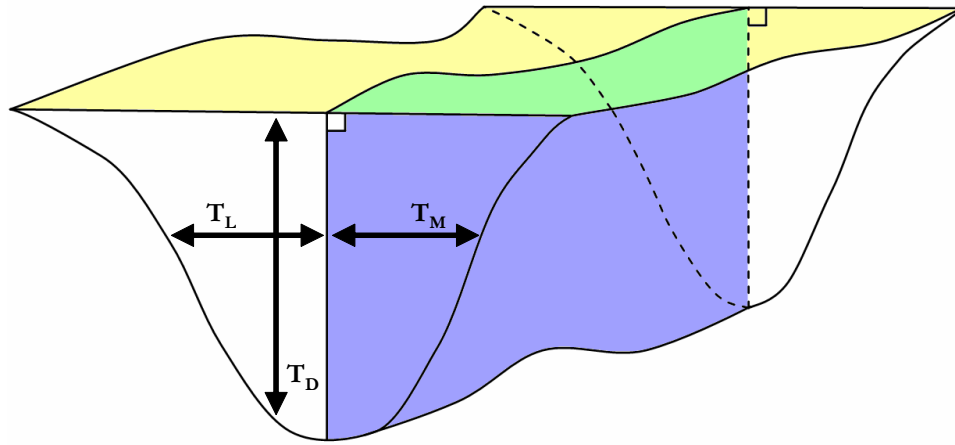


Figure 6. A diagram of a BG in 3D, to illustrate the computation of the thickness fields based on the intertubercular and medial sheets. T_D represents a single thickness value computed for the depth field. Note that depth is measured normal to the intertubercular sheet. T_L and T_M represent thickness values computed for the lateral and medial wall fields, respectively. Note that these thicknesses are measured normal to the medial sheet.

5.4. Computation of the thickness fields

By measuring the thicknesses (distances) between the intertubercular and medial sheets and the BG surface, we obtain several scalar fields (each mapping $\mathbb{R}^2 \rightarrow \mathbb{R}^+$), consisting of these measured thicknesses. For example, referring to figure 6, by computing T_D values at some sampling interval across the entire intertubercular sheet, we obtain a mapping between each sample $(i, j) \in \mathbb{R}^2$ on the intertubercular sheet and a scalar value $T_D \in \mathbb{R}^+$ representing the length of the segment S_D normal to the intertubercular sheet at (i, j) whose endpoints are (1) the point of intersection of S_D and the intertubercular sheet and (2) the point of intersection of S_D and the BG

surface. Similarly, we compute the medial wall field (see T_M in figure 6) and the lateral wall field (see T_L in figure 6); the only difference is that the analogous segments S_M and S_L are normal to the medial sheet, rather than the intertubercular sheet. Note that T_M and T_L need not be equal; this is a deviation from the classical medial axis transform that results in insensitivity to slight changes in the BG walls. The width field is computed to be the sum of the medial and lateral wall fields. The thickness fields can be visualized as 2D grayscale images, where the (x, y) coordinates of each pixel correspond to the (i, j) coordinates of a (medial or intertubercular) sheet sample point, and the intensity at the pixel corresponds to the thickness value to which the field maps (i, j) . Figure 5(f)-(i) shows the depth, width, lateral and medial wall fields visualized in this way, with darker intensity values corresponding to larger thicknesses. These fields are the result of a decomposition of the overall shape of the BG into clinically meaningful parts to facilitate statistical analysis and clinical exploration. The decomposition is a natural result of the choice of medial shape representation. The clinical relevance of each thickness field is discussed in section 6.

6. RESULTS

Qualitative interpretation of the thickness fields is useful to the clinician attempting to examine a single aspect of BG shape (e.g. depth) in isolation. The width field can be used to compute the overall width of the BG, not only at the top between the tuberosities (as it is often computed in related work), but also the width, and the rate of change of the width, throughout the entire depth of the groove. This is useful in determining if a BG narrows sharply towards the inside, which can be a source of irritation to the long biceps tendon. For example, figure 5(g) shows a narrowing of the groove proximal to the shoulder (lighter area on the right).

Similarly, the depth field can be used to determine the maximum depth, but can also be used to determine depth values and their rates of change throughout the BG. This information is useful in assessing the probability of dislocation of the tendon from the BG, and also the tendency of the BG to irritate the tendon (if the BG is deep and narrow). For example, figure 5(f) shows that a distinct deepening of the BG proximal to the shoulder (darker area on the right). Taking this information together with that obtained from the width field, we conclude that the BG becomes both narrow and deep proximal to the shoulder; a condition that warrants attention as it may contribute to tendon irritation if the deepening/narrowing is extreme enough.

The medial and lateral wall fields can be used to assess wall angle and irregularities in the walls. The magnitude of the first derivative of these fields can be used to detect spurs and other abnormalities. In a healthy BG with smooth walls, the first derivative reveals a slow rate of change throughout. Local areas containing high rates of change in intensity (and therefore also in distance to the medial sheet) may be indications of an abnormality, such as a spur.²

To evaluate whether the chosen shape representation captures variability in shape, statistics were computed across bicipital groove shapes collected from 38 different patients. Table 1 shows the results (see caption for details). The standard deviations of the thickness field values are encouraging; they suggest, preliminarily, that intra-class variations in BG shape are captured by these thickness fields, computed relative to the medial sheet and intertubercular sheet.

	<i>Max</i>	<i>Min</i>	<i>Mean</i>	<i>Std. Dev.</i>
<i>Depth (Max, Mean)</i>	(9.16, 2.97)	(2.40, 0.83)	(4.69, 1.94)	(1.26, 0.47)
<i>Width (Max, Mean)</i>	(23.85, 9.73)	(6.30, 3.40)	(15.72, 7.31)	(3.53, 1.33)
<i>Pos. Wall (Max, Mean)</i>	(11.92, 4.89)	(3.15, 1.70)	(7.86, 3.65)	(1.76, 0.66)
<i>Neg. Wall (Max, Mean)</i>	(12.06, 5.37)	(4.28, 1.74)	(8.04, 3.63)	(1.85, 0.76)

Table 1. For each data set, the max. and mean of each thickness field was computed. The max., min., mean, and std. dev. of these quantities was computed across all 38 data sets, with the results shown in this table (units are millimeters).

7. CONCLUSIONS AND FUTURE WORK

In this work, we have provided the motivation for the exploration of a new application of 3D shape description in medical imaging. Medial descriptions of shape allow for the decomposition of shape variations into clinically

relevant parts, for independent qualitative and quantitative exploration and analysis, leading to better diagnosis and injury prediction in musculoskeletal disorders. Applied to the bicipital groove of the proximal humerus, this approach allows for the exploration of all clinically relevant BG shape characteristics: depth, width, slopes and smoothness of wall angles.

The main direction of future work in this area is to design a classifier that uses the shape descriptors developed here to classify a patient according to the malady or injury from which he/she suffers, if any. Design of such a classifier will require more complex statistical analysis of the training data (thickness fields and medial geometry of each BG) to determine the shape characteristics normal and abnormal grooves. Another interesting future investigation based on this work is handedness identification in forensic science, including a comparison of a handedness classifier based on the shape descriptors defined here to previous research in the area.¹⁹

REFERENCES

1. S. R. Aylward, J. Jomier, S. Weeks, and E. Bullitt, "Registration and Analysis of Vascular Images," *IJCV*, **55(2-3)** pp. 123–138, 2003.
2. J. E. Bateman, *The Shoulder and Neck*, W. B. Saunders Company, U.S.A., 1978.
3. H. Blum, "A Transformation for Extracting New Descriptors of Shape," *Models for the Perception of Speech and Visual Form*, W. Whaten-Dunn ed., MIT Press, Cambridge, MA, U.S.A., pp. 362–380.
4. A. F. DePalma, *Surgery of the Shoulder*, J. Lippincott, Philadelphia, U.S.A., 1983.
5. P. Golland and W. E. L. Grimson, "Fixed Topology Skeletons," *CVPR*, **1(1)**, pp. 10–17, 2000.
6. H. H. Hitchcock and C. O. Bechtol, "Painful Shoulder. Observations on the role of the tendon of the biceps brachii in its causation," *J. Bone and Joint Surg., American Volume*, **30A**, pp. 263–273, 1948.
7. A. K. Jain, *Fundamentals of Digital Image Processing*, Prentice Hall, New Jersey, U.S.A., 1989.
8. R. A. Katz and S. M. Pizer, "Untangling the Blum Medial Axis Transform," *IJCV*, **55(2-3)** pp. 139–153, 2003.
9. The MathWorks, Inc., *MATLAB Version 7.0.4.365 (R14) Service Pack 2*, January 2005.
10. A. W. Meyer, "Spontaneous Dislocation and Destruction of Tendon of Long Head of Biceps Brachii. Fifty-nine Instances", *Arch. Surg.*, **17** pp. 493–506, 1928.
11. J. A. Nicholas, E. B. Hershman, and M. A. Posner, *The Upper Extremity in Sports Medicine*, Mosby-Year Book, Inc., U.S.A., 1995.
12. D. O'Donoghue, "Subluxing biceps tendon in the athlete," *Am. J. Sports Med.*, **1(3)**, pp. 20–29, March/April 1973.
13. F. A. Pettrone, *Athletic Injuries of the Shoulder*, McGraw-Hill Inc., U.S.A., 1995.
14. M. Pfahler, S. Brenner, and H. Refior, "The role of the bicipital groove in tendopathy of the long biceps tendon," *J. Shoulder Elbow Surg.*, pp. 419–424, 1999.
15. S. Pizer, P. T. Fletcher, S. Joshi, A. Thall, J. Z. Chen, Y. Fridman, D. S. Fritsch, A. Graham Gash, J. M. Glotzer, M. R. Jiroutek, C. Lu, K. E. Muller, G. Tracton, P. Yushkevich, and E. L. Chaney, "Deformable M-Reps for 3D Medical Image Segmentation," *IJCV*, **55(2-3)** pp. 85–106, 2003.
16. S. Pizer, K. Siddiqi, G. Szekely, J. N. Damon, S. W. Zucker, "Multiscale Medial Loci and Their Properties," *IJCV*, **55(2-3)** pp. 155–179, 2003.
17. D. T. Sandwell, "Biharmonic Spline Interpolation of GEOS-3 and SEASAT Altimeter Data," *Geophysical Research Letters*, **2** pp. 139–142, 1987.
18. D. J. Sartoris, *Principles of Shoulder Imaging*, McGraw-Hill Inc., U.S.A., 1995.
19. K. G. Selvaraj, V. Selvakumarb, I. Indrasinghb, and G. Chandib, "Handedness Identification from Intertubercular Sulcus of the Humerus by Discriminant Function Analysis," *Forensic Sci. International*, **98**, pp. 101–108, 1998.
20. M. Shankman, and S. Beltran, "MRI of the Shoulder," *Curr. Probl. Diagn. Radiol.*, pp. 204–225, November/December 1999.
21. M. Styner, G. Gerig, S. Joshi, and S. Pizer, "Automatic and Robust Computation of 3D Medial Models Incorporating Object Variability," *IJCV*, **55(2-3)** pp. 107–122, 2003.

22. K. Strobel, T.C. Treumann, and B. Allgayer, "Posterior Entrapment of the Long Biceps Tendon After Traumatic Shoulder Dislocation: Findings on MR Imaging," *Am. J. Roentgenol.*, **178(1)** pp. 238–239, January 2002.
23. K. Ueberham and P. Le Floch-Prigent, "Intertubercular Sulcus of the Humerus: Biometry and Morphology of 100 Dry Bones," *Surg. and Radiol. Anat.*, **20(5)**, pp. 351–354, 1998.
24. G. Walch, L. Nov-Josserand, P. Boileau, and C. Levigne, "Subluxations and dislocations of the tendon of the long head of the biceps," *J. Shoulder and Elbow Surg.*, pp. 100–108, 1998.